Supplementary Information for "Promising photovoltaic efficiency of a layered silicon oxide crystal Si_3O"

Sejoong Kim,[1,2,*] Kisung Chae,[2,3,4,†] and Young-Woo Son[2,‡]

[1] *University of Science and Technology (UST), Daejeon 34113, Korea*
[2] *Korea Institute for Advanced Study, Seoul 02455, Korea*
[3] *Department of Chemistry and Biochemistry, University of California, San Diego, CA 92093, United States*
[4] *Materials Science and Engineering Department, The University of Texas at Dallas, Richardson, Texas 75080, United States*

(Dated: June 24, 2020)

I. COMPUTATIONAL DETAILS

We perform the DFT calculations in order to construct mean-field wavefunctions and energy bands for the *GW* calculations. We use the QUANTUM ESPRESSO[1,2] with the plane-wave basis, the PBE exchange-correlation functional[3] and norm-conserving pseudopotentials[4,5]. For the self-consistent calculation, $24 \times 24 \times 1$ and $24 \times 24 \times 4$ k-point grids are adopted for monolayer and bulk respectively. Energy cutoff 952 eV is used for the plane wave expansion. We use the semiemprical Grimme's DFT-D2 scheme[6] for the van der Waal's correction in order to obtain the fully relaxed structure of the layered bulk Si_3O.

The *GW* calculations are performed by using the BERKELEYGW package[7] at the level of G_0W_0 and GW_0. Electronic self-energy is calculated by using the generalized plasmon-pole model[8] and the modified static remainder approach[9]. The convergence of the quasi-particle (QP) band structure are achieved by tuning parameters such as the k-point grid, the energy cutoff of the dielectric matrix $\epsilon^{-1}_{\mathbf{G},\mathbf{G}'}$ and the number of unoccupied bands N_b. The Coulomb interaction truncation scheme[10] is used to simulate the isolated monolayer geometry of Si_3O. Considering that the QP band structure for low-dimensional systems can show a very slow convergence as a function of the size of the vacuum region as reported in Ref. 11, the convergence of the QP band structure is also checked by varying the size of vacuum. The parameters mentioned above are tuned in order to converge the QP energy gap within 50 meV.

We use the energy cutoff 340 eV for the dielectric matrix $\epsilon^{-1}_{\mathbf{G},\mathbf{G}'}$, and $N_b = 1000$ unoccupied bands for mono-layer and bulk of Si_3O. Figure S1 shows the convergence behavior of the QP band gap at the symmetric point Y as a function of the number of unoccupied bands N_b and the energy cutoff of the dielectric function $\epsilon^{-1}_{\mathbf{G},\mathbf{G}'}$. In our calculation $14 \times 14 \times 1$ and $6 \times 6 \times 3$ k-grids are sampled for monolayer and bulk, respectively. We increase the cell size up to 40 Å along the normal direction to the layer plane.

Self-consistently iterative calculations on G are performed to calculate QP band gaps in the so-called GW_0 approximation. It is shown that the corresponding band gaps determined by GW_0 approximation are converged to the QP

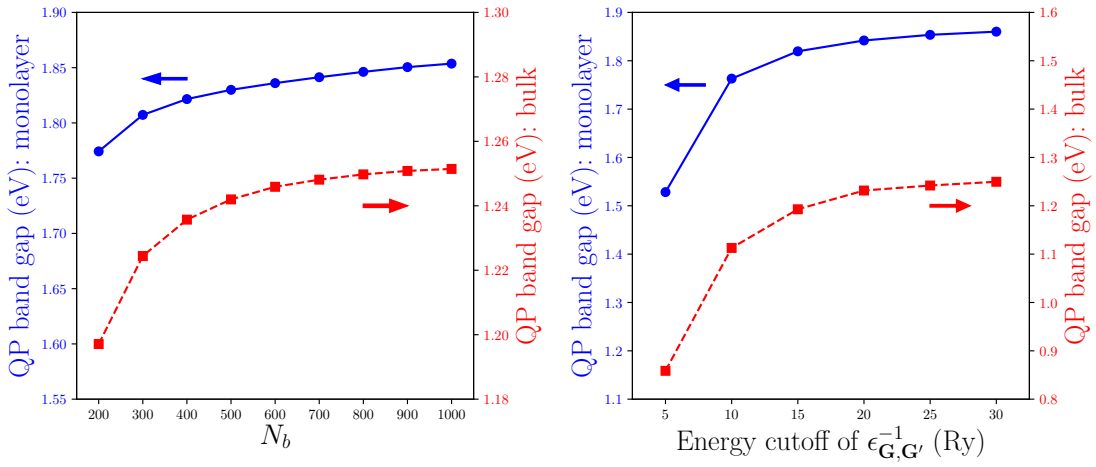

FIG. S1. (Color online) Convergence behaviors of QP band gaps as a function of (a) the number of unoccupied bands N_b and (b) the energy cutoff of the dielectric function $\epsilon^{-1}_{\mathbf{G},\mathbf{G}'}$. QP band gaps of monolayer and bulk Si_3O are indicated by blue solid lines and red dashed lines, respectively.

band gap linearly interpolated from the G_0W_0 gap[8]. Within three iterations the difference between the G_3W_0 gap and the linearly interpolated gap becomes smaller than 5 meV.

We solve the Bethe-Salpeter equation (BSE) with QP energy bands of Si_3O in order to obtain optical absorption spectrum $\epsilon_2(\omega)$ (the imaginary part of the dielectric function) and exciton energy levels. The numerical solution of the BSE depends on the size of k-point mesh and the number of valence and conduction bands. $40 \times 40 \times 1$ and $20 \times 20 \times 4$ k-point grids are used to reproduce well-converged absorption spectra for monolayer and bulk Si_3O, respectively. In our calculation six highest valence bands and six lowest conduction ones are used to solve the BSE, and it is shown that the absorption spectrum is well converged up to about 4.0 eV. Gaussian broadening of 0.05 eV is adopted to numerically calculate the absorption spectrum. The absorption spectrum is calculated on the energy grid whose interval is $\hbar\Delta\omega = 0.01$, on which the numerical integration is performed for the spectroscopic limited maximum efficiency (SLME)[12].

The analytic expression of the absorption spectrum $\epsilon_2(\omega)$ involves the delta function, which can be replaced by the Gaussian function with the broadening parameter in the numerical calculation. The broadening parameter, which is in principle small, is needed to be a finite value suitable to numerical integrations for $\epsilon_2(\omega)$ and the SLME η, which are based on the **k**-point mesh and the discrete grid of ω. If the broadening parameter is smaller than the energy resolution of the integration, the spectrum $\epsilon_2(\omega)$ shows spurious and bumpy features due to the finite sampling. In contrast, too large smearing parameter can wash out important detailed features of the spectrum. We have tested the effect of broadening parameters for $\epsilon_2(\omega)$ on SLME calculations. The calculations show that the SLME η maintains about 26–27% within the range from 0.02 to 0.06. If the smearing parameter is smaller than the energy resolution $\hbar\Delta\omega = 0.01$ eV, or it is much larger (> 0.08 eV), the SLME η deviates from 26–27% as shown in Fig S2(b).

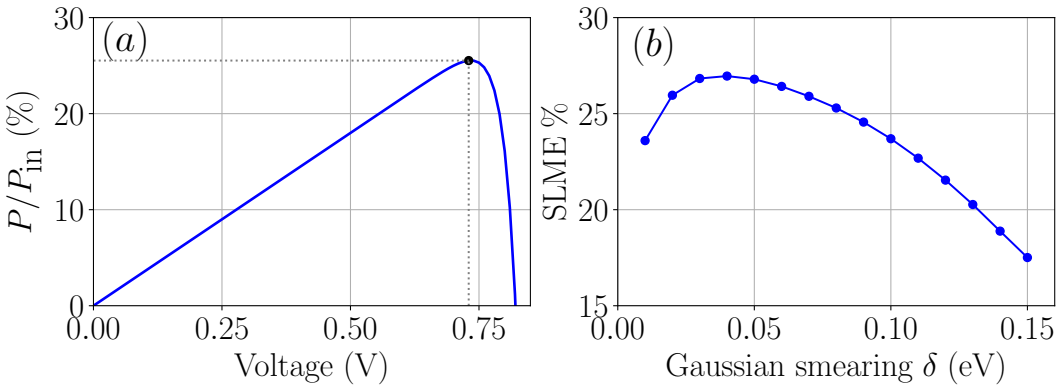

FIG. S2. (Color online) (a) P/P_{in} (blue solid line) as a function of the voltage V. The SLME η, the maximum value of P/P_{in}, is indicated by black circle. (b) SLME η calculations by tuning the broadening parameter from 0.01 to 0.15.

II. SLME CALCULATIONS

The SLME η of the solar cell can be calculated by maximizing the ratio P/P_{in}[12,13]. Here the total incident solar energy density P_{in} is calculated by using the Air Mass 1.5 data[14] for the solar irradiance spectrum of the photon flux $I_{AM1.5}(E)$,

$$P_{in} = \int_0^\infty I_{AM1.5}(E) E dE. \tag{1}$$

The output power density of the solar cell P is the product of the total net current density J and the voltage V,

$$P = JV = \left[J_{sc} - J_0 \left(e^{eV/k_BT} - 1 \right) \right] V, \tag{2}$$

where e, k_B, and T are the electron charge, the Boltzmann constant, and the solar cell temperature, respectively[12,13]. The net current density J is determined by two contributions: the short-circuit current density J_{sc} and the reverse saturation current density J_0. The short-circuit current density J_{sc} is calculated from the absorbance $A(E)$ and the

AM1.5 spectrum $I_{AM1.5}(E)$,

$$J_{sc} = e\int_0^\infty A(E)I_{AM1.5}(E)dE. \tag{3}$$

J_0 is further expressed as the sum of the non-radiative electron-hole combination current density J_0^{nr} and the radiative one J_0^r,

$$J_0 = J_0^{nr} + J_0^r = \frac{J_0^r}{f_r}. \tag{4}$$

Here $f_r = J_0^r/(J_0^{nr} + J_0^r)$ is the fraction of the radiative combination current, which is approximately given by $f_r = e^{-(E_g^{da}-E_g)/k_BT}$, where E_g and E_g^{da} are the minimum gap and the directly allowed gap, respectively[12,13]. Considering the principle of the detailed balance, the radiative combination current J_0^r is equal to the absorption rate of photons from the surrounding thermal path in equilibrium with the solar cell surface:

$$J_0^r = e\pi\int_0^\infty A(E)I_{bb}(E,T)dE, \tag{5}$$

where $I_{bb}(E,T)$ stands for the spectrum of the black body at temperature T,

$$I_{bb}(E,T) = \frac{2\pi}{h^3c^2}\frac{E^2}{e^{E/k_BT}-1}, \tag{6}$$

where h and c are the Planck constant and the speed of light, and the temperature of the surrounding thermal bath is $T = 25°C$ in this work. The SLME η can be obtained by numerically maximizing P as shown in Fig. S2(a).

III. THERMAL STABILITY OF Si_3O

Here, *ab initio* molecular dynamics (AIMD) is employed to show robust thermal stability of Si_3O in addition to convex Hull and harmonic phonon dispersion provided in Ref. 15. The Si_3O monolayer is expanded to a (3×3×1) supercell which contains 18 Si_3O formula units. AIMD is performed at a temperature of 1,500 K in canonical ensemble (i.e., constant NVT), where temperature of the system is controlled by Nosé-Hoover thermostat. The system is integrated by using Verlet algorithm for 10 pico seconds (or 10,000 steps) with a time step of 1 femto second. Fig. S3 shows temporal evolution of energy and temperature of the system during the AIMD calculation. The instantaneous energy seems to fluctuate around a constant value within a reasonable energy window, indicating that the temporal

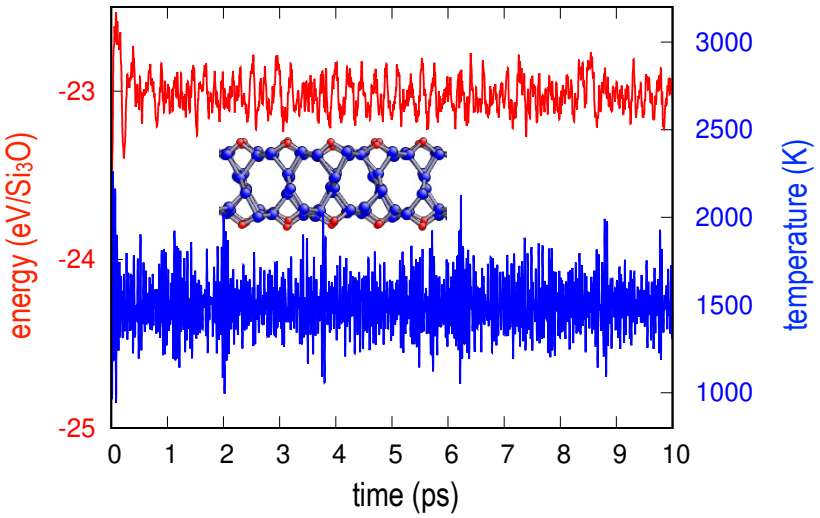

FIG. S3. (Color online) Evolution of energy (red) and temperature (blue) with elapsed time. Snapshot of Si_3O is shown in the inset.

average is kept constant. This means that the atomic arrangements in the Si_3O remain stable without any broken bonds throughout the AIMD calculations. The inset in Fig. S3 shows a snapshot of the Si_3O monolayer during the AIMD. Each of the atoms vibrates at their equilibrium positions due to the kinetic energy, but the initial structure is maintained, confirming the robust thermal stability.

IV. EFFECTIVE MASSES IN Si_3O

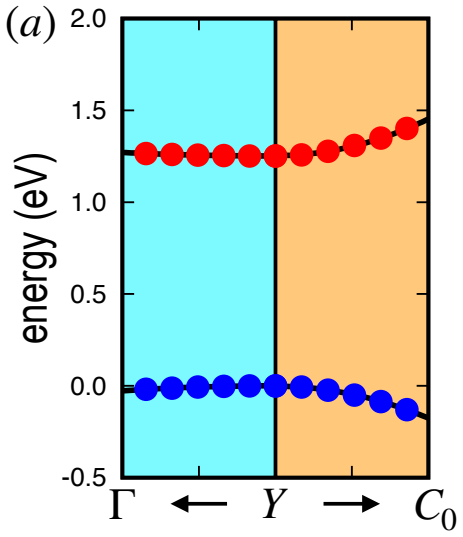

(b)

direction	carrier	
	hole	electron
Y→Γ	0.22 m_0	0.32 m_0
Y→C_0	0.035 m_0	0.031 m_0

FIG. S4. (Color online) Effective masses of Si_3O. (a) Quasiparticle eigenvalues near the band edges: conduction (red symbols) and valence (blue symbols) bands along Y-Γ (cyan shading) and Y-C_0 (orange shading) directions. The black curves behind the data points are fitted to quadratic functions. (b) The calculated effective masses are tabulated relative to an electron rest mass m_0.

Carrier mobility (μ) is an important characteristic in photovoltaic applications for efficient charge separation and photo-current collection. In solids, the carrier mobility can be shown as

$$\mu = \frac{q\tau}{2m^*}$$

where q is an elemental charge, τ is scattering time and m^* is an effective mass. The scattering time τ depends on various factors such as details of electronic structures, defect concentrations and temperature, and electron-phonon scattering becomes a dominant factor for pure bulk materials with few defects. While elaborated evaluation of the τ is crucial for the quantitatively assessment of carrier mobility, it will require demanding computation of electron-phonon coupling matrix, which is beyond the scope of this paper. As a crude approximation, we hypothesize that effective masses (m^*) be sufficient to possibly show qualitative picture of carrier mobility behaviors in Si_3O. We investigate the in-plane effective masses in bulk Si_3O from quasiparticle band structures as shown in Fig. 2(b). Two high-symmetry paths are considered: from Y to Γ and from Y to C_0, and small fractions of each path around the Y momentum, where both maximum and minimum occur, are shown in Fig. S4(a). Quasiparticle eigenvalues along each of the paths in each band are used to separately fit the harmonic energy-momentum (E-k) dispersion behavior near the band edges, i.e.,

$$E(k) = E_0 + \frac{\hbar k^2}{2m^*}$$

where $\hbar$ is Planck constant. The effective mass can be obtained from the curvature of the second derivative of the band structure,

$$(m^*)^{-1} = \frac{1}{\hbar}\frac{d^2E}{dk^2}$$

which is usually used relative to the electron rest mass m_0. Figure S4(b) shows the m^* for each direction and for both electron and hole. It is interesting that the effective masses for both electron and hole along different directions show an order-of-magnitude difference, indicating that the Si_3O is highly anisotropic. Moreover, the effective mass values of the *light* bands for both electron and hole are remarkably small ($\sim$0.03 m_0), comparable to well-known high mobility semiconductors such as InSb (0.0135 m_0) and GaAs (0.067 m_0)[16]. Even for the *heavy* bands, the effective mass values are comparable to a bulk silicon crystal (0.19 m_0 and 0.16 m_0 for electron and hole, respectively). It is worth noting that the band edges at Y serve as the sole predominant inter-band transition path across the band gap up to a few hundreds meV, limiting the number of possible electron-phonon coupling pathways up to considerable temperature range. With remarkably small effective masses for both electron and hole as well as the interesting electronic structures favorable for efficient carrier transport, Si_3O makes a promising candidate for photovoltaic applications.

---

* E-mail: sejoong@ust.ac.kr
† E-mail: kisung@kias.re.kr
‡ E-mail: hand@kias.re.kr

[1] P. Giannozzi, O. Andreussi, T. Brumme, O. Bunau, M. Buongiorno Nardelli, M. Calandra, R. Car, C. Cavazzoni, D. Ceresoli, M. Cococcioni, N. Colonna, I. Carnimeo, A. Dal Corso, S. de Gironcoli, P. Delugas, R. A. DiStasio Jr, A. Ferretti, A. Floris, G. Fratesi, G. Fugallo, R. Gebauer, U. Gerstmann, F. Giustino, T. Gorni, J Jia, M. Kawamura, H.-Y. Ko, A. Kokalj, E. Kücükbenli, M. Lazzeri, M. Marsili, N. Marzari, F. Mauri, N. L. Nguyen, H.-V. Nguyen, A. Otero de-la Roza, L. Paulatto, S. Poncé, D. Rocca, R. Sabatini, B. Santra, M. Schlipf, A. P. Seitsonen, A. Smogunov, I. Timrov, T. Thonhauser, P. Umari, N. Vast, X. Wu, and S. Baroni, J. Phys.: Condens. Matter **21**, 395502 (2009).

[2] P. Giannozzi, S. Baroni, N. Bonini, M. Calandra, R. Car, C. Cavazzoni, D. Ceresoli, G. L. Chiarotti, M. Cococcioni, I. Dabo amd A. Dal Corso, S. Fabris, G. Fratesi, S. de Gironcoli, R. Gebauer, U. Gerstmann, C. Gougoussis, A. Kokalj, M. Lazzeri, L. Martin-Samos, N. Marzari, F. Mauri, R. Mazzarello, S. Paolini, A. Pasquarello, L. Paulatto, C. Sbraccia, S. Scandolo, G. Sclauzero, A. P. Seitsonen, A. Smogunov, P. Umari, and R. M. Wentzcovitch, J. Phys.: Condens. Matter **29**, 465901 (2017).

[3] J. P. Perdew, K. Burke, and M. Ernzerhof, "Generalized gradient approximation made simple," Phys. Rev. Lett. **77**, 3865 (1996).

[4] D. Hamann, M. Schlüter, and C. Chiang, "Norm-conserving pseudopotentials," Phys. Rev. Lett. **43**, 1494–1497 (1979).

[5] G. Bachelet, D. Hamann, and M. Schlüter, "Pseudopotentials that work: From h to pu," Phys. Rev. B **26**, 4199–4228 (1982).

[6] S. Grimme, "Semiempirical gga-type density functional constructed with a long-range dispersion correction," J. Comp. Chem. **27**, 1787 (2006).

[7] J. Deslippe, G. Samsonidze, D. A. Strubbe, M. Jain, M. L. Cohen, and S. G. Louie, "Berkeleygw: A massively parallel computer package for the calculation of the quasiparticle and optical properties of materials and nanostructures," Comput. Phys. Commun. **183**, 1269 (2012).

[8] M. Hybertsen and S. Louie, "Electron correlation in semiconductors and insulators: Band gaps and quasiparticle energies," Phys. Rev. B **34**, 5390–5413 (1986).

[9] J. Deslippe, G. Samsonidze, M. Jain, M. L. Cohen, and S. G. Louie, "Coulomb-hole summations and energies for *gw* calculations with limited number of empty orbitals: A modified static remainder approach," Phys. Rev. B **87**, 165124 (2013).

[10] S. Ismail-Beigi, "Truncation of periodic image interactions for confined systems," Phys. Rev. B **73**, 233103 (2006).

[11] D. Y. Qiu, F. H. da Jornada, and S. G. Louie, "Optical spectrum of MoS_2: Many-body effects and diversity of excition states," Phys. Rev. Lett. **111**, 216805 (2013).

[12] L. Yu and A. Zunger, "Identification of potential photovoltaic absorbers based on first-principles spectroscopic screening of materials," Phys. Rev. Lett. **108**, 068701 (2012).

[13] Kamal Choudhary, Marnik Bercx, Jie Jiang, Ruth Pachter, Dirk Lamoen, and Francesca Tavazza, "Accelerated discovery of efficient solar cell materials using quantum and machine-learning methods," Chemistry of Materials **31**, 5900–5908 (2019).

[14] "Reference solar spectral irradiance: Air mass 1.5," https://rredc.nrel.gov/solar//spectra/am1.5/.

[15] Kisung Chae and Young-Woo Son, "A new family of two-dimensional crystals: Open-framework T_3X (T = C, Si, Ge, Sn; X = O, S, Se, Te) compounds with tetrahedral bonding," Nano. Lett. **19**, 2694–2699 (2019).

[16] I. Vurgaftman, J. R. Meyer, and L. R. Ram-Mohan, "Band parameters for iii–v compound semiconductors and their alloys," Journal of Applied Physics **89**, 5815–5875 (2001).